Development and Implementation of CAE System "HEARTS" for Heat Treatment Simulation Based on Metallo-Thermo-Mechanics

T. Inoue and K. Arimoto

Based on the framework of "metallo-thermo-mechanics" proposed by the authors, a CAE system, "HEARTS" (HEAt tReaTment Simulation system), has been developed to simulate metallic structure, temperature, and stress/strain in the heat treatment processes associated with phase transformation, such as quenching and tempering by means of the finite element method. In the first part of the paper, the governing theory is introduced; fundamental equations of metallurgical change due to phase transformation, heat conduction, and stress analysis are presented; and the effect of coupling among these three fields is discussed. The development strategy, methodology, structure, and directions for use of the HEARTS system are stated in the following sections. Simulated results on temperature, structural change, and stress/strain, as well as carbon content during the heat treatment process, are illustrated for engineering components in two- and three-dimensional shape and a Japanese sword by use of the system combined with a pre-/post-processor. The validity of the system is evaluated by comparison with the experimental data.

Keywords
CAE system, carburization, finite element method, heat treatment, metallo-thermo-mechanics, quenching, tempering

1. Introduction

COMPUTER SIMULATION is indispensable for research, development, and design in various fields of industry. In particular, popularization of general-purpose programs based on the finite element method has enabled engineers to execute highly reliable analysis and design. However, many problems remain to which the general-purpose programs cannot be applied. Heat treatment associated with phase transformation is one example, and the development of a program specialized for heat treatment simulation is required from an engineering point of view.

Owing to the fact that metallic structures, temperature, and stress/strain are strongly coupled in the process incorporating phase transformation, a metallo-thermo-mechanics theory for considering the coupling effect was proposed and applied to some problems by the authors (Ref 1-7).

In the first part of the paper, the metallo-thermo-mechanics theory is briefly introduced; governing equations to identify the fields of metallic structure, temperature, and stress/strain are discussed; and the correlation between the problems of phase transformation and the theory is considered. In the following sections, the development strategy, methodology, structure, and directions for use of the HEARTS (HEAt tReaTment Simulation system) based on the theory for simulating the engineering process incorporating phase transformations are stated.

Simulated results are presented: a long cylinder quenched by water, a carburizing-quenched gear wheel, an induction-quenched and tempered ring, and a Japanese sword quenched by water. The theory and the system are evaluated by comparison between simulated results and experimental data.

T. Inoue, Department of Energy Conversion Science, Kyoto University, Sakyo-ku, Kyoto 606-01, Japan; and **K. Arimoto,** CRC Research Institute, Inc., Chuo-ku, Osaka 541, Japan.

2. Summary of Metallo-Thermo-Mechanics

2.1 *Coupling Effects in the Processes Incorporating Phase Transformations*

In many engineering processes incorporating phase transformations such as quenching, tempering, welding, and casting, the metallic structures of steel are transformed, for example, from pearlite or ferrite to austenite in the heating process, and form austenite to martensite or pearlite in the cooling process. The distribution of temperature and stress/strain are also altered during the course, and the three fields affect each other (Ref 1-7) as schematically illustrated in Fig. 1. These effects are termed "metallo-thermo-mechanical coupling" (Ref 6, 7) by the authors. The coupling effects are indicated by arrows in Fig. 1:

1. *Thermal stress:* In heat treatment processes, a significant temperature gradient is generated in the work. The thermal expansion caused by such a temperature gradient is restricted by the shape of a solid body, thus generating thermal stress.
2. *Heat generation due to deformation:* When stress/strain is applied to a solid, the energy is partially discharged as heat. In the case of inelastic deformation, the heat generation sometimes reaches a level too high to be ignored.
3. *Temperature-dependent phase transformation:* Temperature is the major factor which determines phase transformation start time. However, in the case of diffusion-type transformations of ferrite, pearlite, and bainite, the temperature history also affects the phase transformation.

4. *Latent heat due to phase transformation:* Latent heat generated in the course of phase transformation affects the temperature field.
5. *Transformation stress and transformation plasticity:* Volume dilatation in the work is caused by the phase transformations. When this volumetric dilatation is inhomogeneous depending on the complicated shape of the body, stress and strain are induced, termed transformation stress and strain. The level of such induced stress is comparable to the thermal stress. The effect of transformation plasticity is sometimes important.
6. *Stress-induced transformation:* The phase transformation behavior is also affected by stress/strain existing in the solid. For example, pearlite transformation time is shortened under tensile stress, and vice versa. Martensite transformation is generated even though a material is processed at temperature higher than the martensite transformation start temperature under the applied stress.

In the cases of carburizing quenching, as shown by the dotted lines in Fig. 1, the distribution of diffused carbon influences the temperature and stress/strain through the variation of material properties. A time-temperature-transformation (T-T-T) diagram and a continuous-cooling-transformation (C-C-T) diagram for steels with different carbon contents are to be used as the fundamental data.

2.2 *Kinetics of Phase Transformations*

The phase transformations during heat treatment processes are classified into diffusion-type and diffusionless-type transformations. Austenite-ferrite and -pearlite structure changes and vice versa are governed by the diffusion-type transformation, which is controlled by temperature history as well as temperature itself. During tempering accompanied by stress relaxation by creep effect, the diffusion-type transformation is also assumed to control the precipitation of carbon-oxide from martensite. The diffusionless-type transformation is, on the other hand, essential for the martensite transformation from austenite.

The Johnson-Mehl equation (Ref 8), one of the most popular kinetic equations, is applied for evaluating volume fractions ξ_I of austenite, pearlite, and bainite in our program. In case of the diffusion-type transformation, experimental results have been accumulated in the form of T-T-T or time-temperature-austenitizing (T-T-A) diagrams. To use these diagrams and consider the effect of stress and carbon content, the following modification of the Johnson-Mehl equation for the volume fraction at time t with a time parameter T is recommended:

$$\xi_I = 1 - \exp\left\{-\int_0^t f_T(T) f_S(\sigma_{ij}) f_C(C)(t-\tau)^3 d\tau\right\} \quad \text{(Eq 1)}$$

This kinetic equation is called the specialized KJMA equation (Kolmogorov-Jonson and Mehl-Avrami equation). In this equation, $f_T(T)$, $f_S(\sigma_{ij})$, and $f_C(C)$ are the functions of temperature T, stress σ_{ij}, and carbon content C, respectively.

In the tempering processes, low-carbon martensite and ε-carbide are produced from martensite in stage 1 in the temperature range 80 to 180 °C, the retained austenite transforms to bainite in stage 2 in the temperature range 230 to 280 °C, and the low-carbon martensite is decomposed into ferrite and cementite in stage 3 in the temperature range 260 to 360 °C. In our program, the temperature-dependent volume fraction induced by these reactions is evaluated by the equation in the first approximation:

$$\xi_J = 1 - \exp\left\{A\left(\frac{T - T_S}{T_e - T_S}\right)^D\right\} \quad \text{(Eq 2)}$$

where T_S and T_e are the transformation start and end temperatures, respectively, and A and D are coefficients set by dilatation-temperature diagrams.

The volume fraction of diffusionless-type transformation dependent on temperature, stress, and carbon content is introduced by modifying Magee's equation (Ref 9) in using the thermodynamic consideration. Therefore the volume fraction of martensite ξ_M is obtained by:

$$\xi_M = 1 - \exp\left\{\psi_1 T + \psi_2(C - C_0) + \psi_{31}\sigma_{ij} + \psi_{32} J_2^{1/2} + \psi_4\right\} \quad \text{(Eq 3)}$$

as the function of carbon content, temperature, and stress. Here, $J_2^{1/2}$ is the second invariant of deviatoric stress. When the martensite transformation start temperatures under carburized conditions and applied stress are given, ψ_2/ψ_1, ψ_{31}/ψ_1, and ψ_{32}/ψ_1 can be determined, and ψ_1 and ψ_4 are identified, if temperatures for martensite-start T_{MS} and for 50% martensite T_{M50} at $\xi_M = 0$ and $\xi_M = 0.5$ are provided, respectively.

The volume fraction of each metallic structure is used to estimate the material parameters χ such as thermal conductivity, specific heat, Young's modulus, yield stress, and hardening modulus during the processes by the mixture law:

$$\chi = \sum \chi_I \xi_I \quad \text{(Eq 4)}$$

in terms of the parameter χ_I of the I-th constituent.

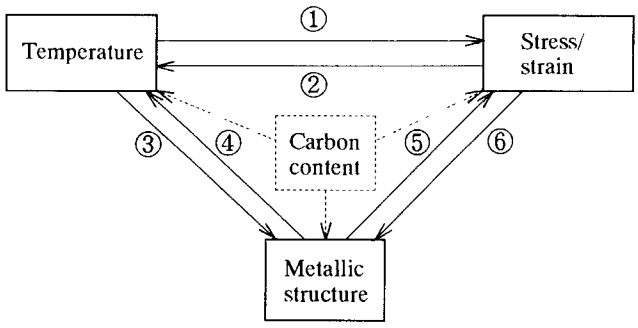

Fig. 1 Metallo-thermo-mechanical coupling. Key: 1, thermal stress; 2, heat generation due to deformation; 3, temperature-dependent phase transformation; 4, latent heat due to phase transformation; 5, transformation stress and transformation plasticity; 6, stress-induced transformation

2.3 *Heat Conduction Equation*

The temperature field during heat treatment is affected by the latent heat due to phase change and also the heat generation converted from mechanical work. So, the heat conduction equation is to be derived by considering the total energy balance, or on the basis of the first law of thermodynamics as:

$$\rho \dot{e} = \sigma_{ij} \dot{\varepsilon}_{ij} - \frac{\partial h_i}{\partial x_i} \quad \text{(Eq 5)}$$

in terms of internal energy $e = g + T\eta + \sigma_{ij}\varepsilon_{ij}/\rho$, with the Gibbs free energy, g, the stress power, $\sigma_{ij}\dot{\varepsilon}_{ij}$, the entropy η, the density π, and the heat flux h_i. Here x_i is a coordinate. Introducing the definition of specific heat $c = T\partial\eta/\partial T$, Eq 5 is reduced to:

$$\rho c \dot{T} - \frac{\partial}{\partial x_i}\left(k\frac{\partial T}{\partial x_i}\right) - \sigma_{ij}\dot{\varepsilon}^p_{ij} + \sum \rho_l l_l \dot{\xi}_l = 0 \quad \text{(Eq 6)}$$

where k and l_l denote the coefficient of heat conduction and the latent heat produced by the progressive l-th constituent with volume fraction ξ_l, respectively.

2.4 *Elastic-Plastic Constitutive Equation*

In this case of infinitesimal deformation, the total strain rate is divided into elastic (e), plastic (p), and thermal (T) strain rates and those by structural dilatation due to phase transformation (m) and transformation plasticity (tp), such that:

$$\dot{\varepsilon}_{ij} = \dot{\varepsilon}^e_{ij} + \dot{\varepsilon}^p_{ij} + \dot{\varepsilon}^T_{ij} + \dot{\varepsilon}^m_{ij} + \dot{\varepsilon}^{tp}_{ij} \quad \text{(Eq 7)}$$

Elastic strain ε^e_{ij} is derived as the function of stress σ_{ij}:

$$\varepsilon^e_{ij} = \frac{1+\nu}{E}\sigma_{ij} - \frac{\nu}{E}\sigma_{kk}\delta_{ij} \quad \text{(Eq 8)}$$

where E is Young's modulus, and ν is Poisson's ratio.

Thermal strain rate ε^T_{ij} is:

$$\varepsilon^T_{ij} = \alpha(T - T_0)\delta_{ij} \quad \text{(Eq 9)}$$

where α is the thermal expansion coefficient.

When introducing temperature- and structure-dependent yield function with the hardening parameter χ.

$$F = F(\sigma_{ij}, \varepsilon^p_{ij}, \kappa, T, \xi_l) \quad \text{(Eq 10)}$$

plastic strain rate $\dot{\varepsilon}^p_{ij}$ is reduced to the form

$$\dot{\varepsilon}^p_{ij} = \Lambda\frac{\partial F}{\partial \sigma_{ij}} = \hat{G}\left(\frac{\partial F}{\partial \sigma_{kl}}\dot{\sigma}_{kl} + \frac{\partial F}{\partial T}\dot{T} + \sum\frac{\partial F}{\partial \xi_l}\dot{\xi}_l\right)\frac{\partial F}{\partial \sigma_{ij}} \quad \text{(Eq 11)}$$

where the hardening function $\hat{G}$:

$$\frac{1}{\hat{G}} = -\left(\frac{\partial F}{\partial \varepsilon^p_{mn}} + \frac{\partial F}{\partial \kappa}\sigma_{mn}\right)\frac{\partial F}{\partial \sigma_{mn}} \quad \text{(Eq 12)}$$

Either the isotropic or kinematic hardening rule by Prager is available to be used in the code.

Strain rates due to phase transformation and transformation plasticity, $\dot{\varepsilon}^m_{ij}$ and $\dot{\varepsilon}^{tp}_{ij}$, depend on the l-th constituent (Ref 10):

$$\dot{\varepsilon}^m_{ij} = \sum \beta_l \dot{\xi}_l \delta_{ij} \quad \text{(Eq 13)}$$

and

$$\dot{\varepsilon}^{tp}_{ij} = \frac{3}{2}\sum K_l h(\xi_l)\dot{\xi}_l s_{ij} \quad \text{(Eq 14)}$$

where

$$h(\xi_l) = 2(1 - \xi_l) \quad \text{(Eq 15)}$$

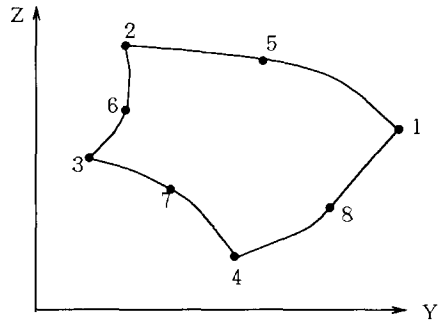

(a)

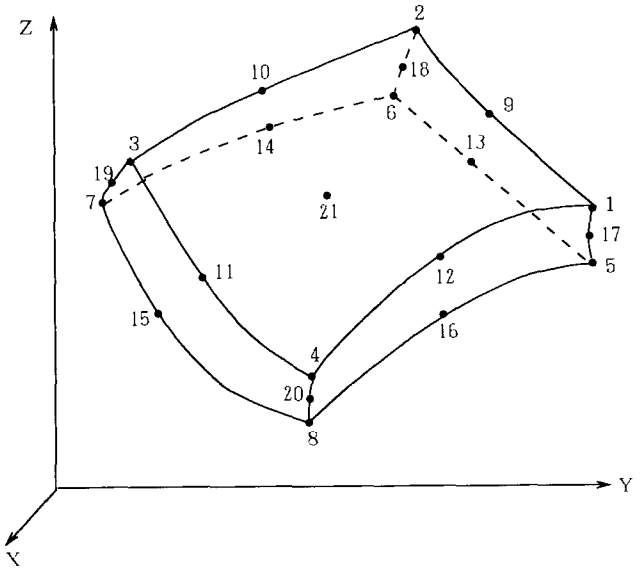

(b)

Fig. 2 Finite elements available in the HEARTS system. (a) 2-D element. (b) 3-D element

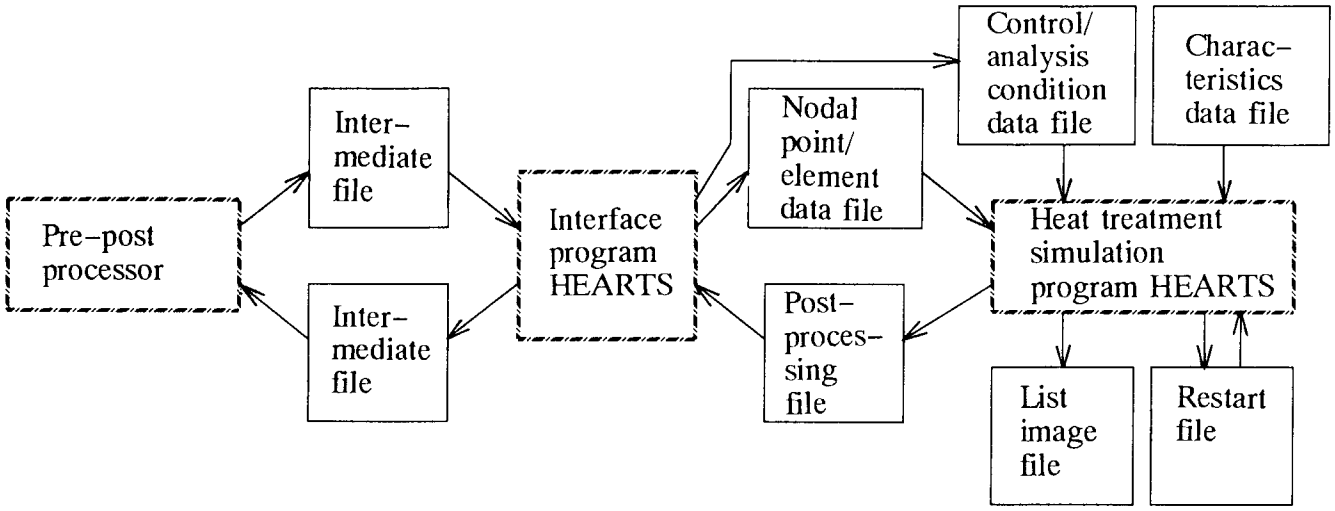

Fig. 3 CAE environment

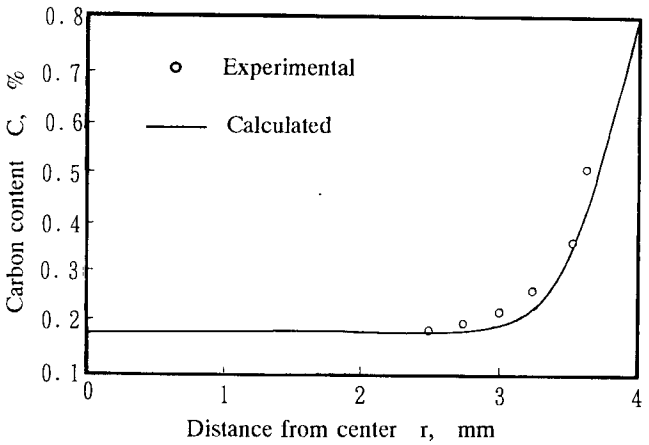

Fig. 4 Distribution of carbon content in the cylinder

and where s_{ij} is deviatoric stress, β_I is the dilatation due to structural change, and K_I is the intensity of transformation plasticity. When creep effect is significant, say in the case of a tempering process, the creep strain rate $\dot{\varepsilon}^c_{ij}$:

$$\dot{\varepsilon}^c_{ij} = \frac{3}{2}\frac{\dot{\bar{\varepsilon}}^c}{\bar{\sigma}} s_{ij} \qquad \text{(Eq 16)}$$

is added to Eq 7, where $\dot{\bar{\varepsilon}}^c$, $\bar{\sigma}$, and s_{ij} are the equivalent creep strain rate, equivalent stress, and deviatoric stress, respectively.

By introducing the constitutive equations into the finite element equation, the stress and strain/deformation can be determined.

2.5 *Diffusion Equation of Carbon*

For the simulation of carburized quenching, normally performed before quenching, it is necessary to solve the diffusion equation, a simpler form of Eq 6:

$$\frac{\partial C}{\partial t} = D\frac{\partial^2 C}{\partial x_I \partial x_J} \qquad \text{(Eq 17)}$$

in order to determine the distribution of carbon content. The diffusion constant generally depends on temperature, carbon content, stress/strain, and volume fraction of each structure.

3. Implementation and Environment of the CAE System

3.1 *Implementation for the Finite Element Method*

The series of equations governing the heat treatment process developed above are to be numerically solved by the finite element method. The finite elements available for the HEARTS system are two- and three-dimensional, as illustrated in Fig. 2. The 2-D element in Fig. 2(a) is converted to a triangular element by overlapping three nodes, for example, No. 1, 2, and 5, and other 3-D elements are easily generated by joining the three nodes located on the corner in Fig. 2(b). The continuum elements are used in the analyses of heat conduction, stress/strain, and diffusion. The 2-D element in Fig. 2(a) is also applied to axisymmetrical problems. For stress/strain analysis, a plane stress/strain problem and a generalized plane strain problem are also available.

The HEARTS system was designed based on the implementation procedure for the finite element technique developed by K.J. Bathe (Ref 11). This procedure is proposed for developing a program for practical use which can analyze very large systems and add some different types of elements and kinds of function without difficulty.

3.2 *Procedure to Solve Coupled Problem*

In this case of the coupled analysis of time-dependent metallic structure, temperature, and stress/strain, a step-by-step method with very short-enough time step is employed to avoid

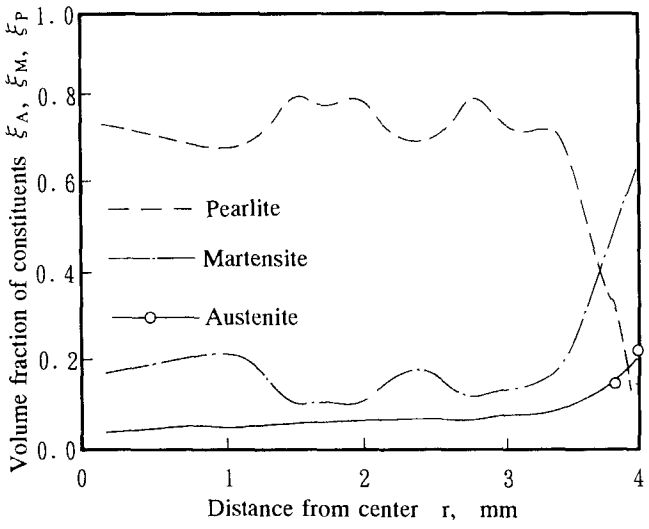

(a)

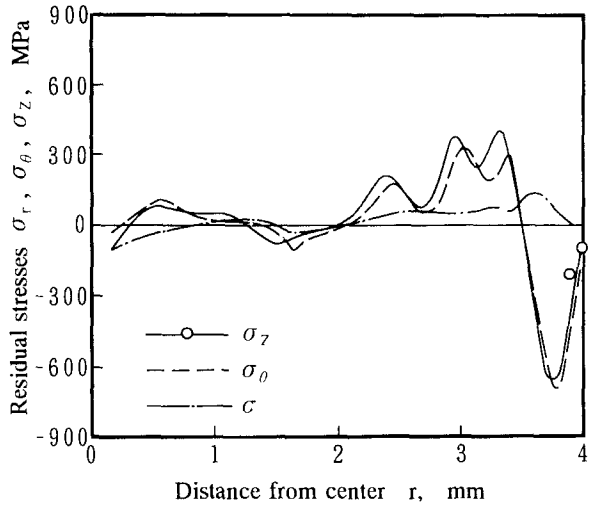

(b)

Fig. 5 Distribution of metallic structures and residual stresses in the cylinder. (a) Austenite, martensite, and pearlite. (b) Residual stresses

the increase of memory due to nonsymmetric matrix and also to reduce execution time.

The heat conduction analysis is carried out by taking into account the latent heat generation calculated by microstructural evolution analysis, followed by the stress/strain analysis, which depends on the structural distribution based on the temperature distribution determined. When the stress/strain analysis comes to the end, calculation in the next step is carried out. When the coupling effect is negligible, independent analysis of the three fields is possible.

The time integration in the heat conduction and diffusion analyses employs the α-method (Ref 11), which is reduced to the trapezoid and Euler backward methods in special cases. Nonlinear equations in each analysis are made by Newton's iteration method.

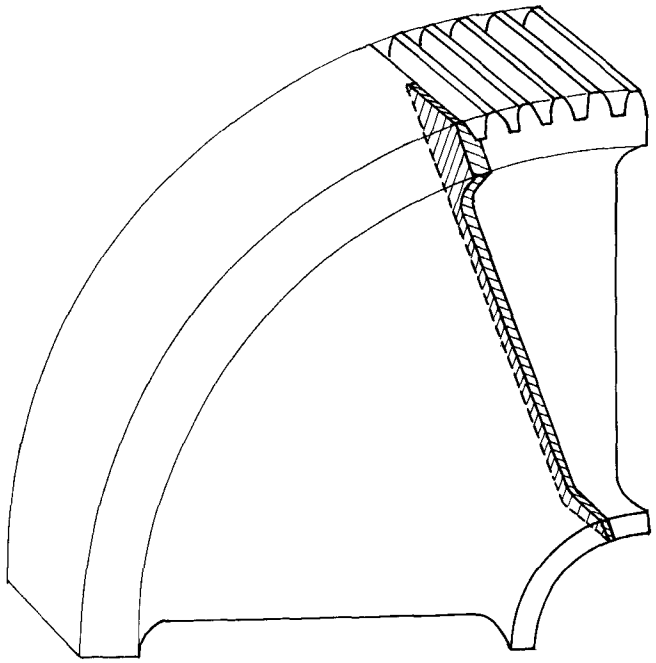

Fig. 6 Shape of a gear with boss

3.3 *CAE Environment*

As shown in Fig. 3, the HEARTS system was developed to be used in the CAE environment combined with a proper pre-/post-processor. The system is designed for exchanging data between a solver and a pre-/post-processor: PATRAN and I-DEAS.

Data necessary for the simulation are created by a pre-/post-processor. These data are output in the format of an "intermediate file," then converted into a "control/analysis condition data file"and a "nodal point/element data file" by an interface program. In addition, input data regarding the characteristics of the elements are made by users in the form of a "characteristics data file."

The results of calculation by the solver are output in such forms as a "post-processing file," "list image file," and "restart file." The contents of the post-processing file are converted to the form of the intermediate file through the interface. The resulting data contained in the intermediate file can be displayed in various forms by using the pre-/post-processor according to the instructions of the users.

4. Simulated Results

The validity of the HEARTS system developed so far for the heat treatment simulation is now evaluated by application to some practical problems. Some results are compared with experimental data.

4.1 *Carburized Water Quenching of a Cylinder*

The first example is the carburized water quenching of a long cylinder of a case-hardening steel containing molybdenum. The cylinder of 8 mm diameter is treated by modeling into a series of elements in the radial direction and by apply-

ing the generalized plane-stress condition for the stress/strain analysis. Temperature-dependent material data necessary for heat conduction and stress/strain analyses are piled up in the material data file.

The solid line in Fig. 4 represents the distribution of carbon content after carburization, which agrees fairly well with data measured by the X-ray diffraction technique, indicated by the circles. Figures 5(a) and (b) are the volume fraction of metallic structures and residual stress distributions, respectively.

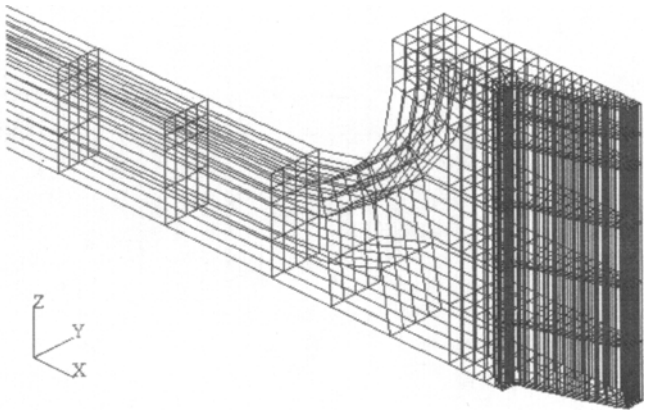

Fig. 7 Mesh division near a tooth

4.2 *Carburized Oil Quenching of a Gear*

Carburized quenching of a gear, shown in Fig. 6, is the second example. The gear is an involute type with a pressure angle of 20°, 90 teeth, 3 modules, 277.11 mm outer diameter, and 40 mm tooth width. Figure 7 illustrates the mesh division of the part, which constitutes the entire wheel by overlapping itself on the inclined faces. The numbers of nodal points and elements of the model are 1,369 and 932, respectively, and an 8-nodal-point isoparametric element is used.

The material is a nickel-chromium steel. The carburizing process consists of a 210 min carburizing stage and a 63 min diffusion stage. The boundary conditions for carburization of carbon are assumed such that no carbon diffusion occurs from the external environments via the radial surfaces on the tip and bottom of the tooth. It is also assumed in the carburizing stage that the carbon content in external environments is 1.0% for 0 to 120 min and 0.8% for 120 to 210 min. Furthermore, in the

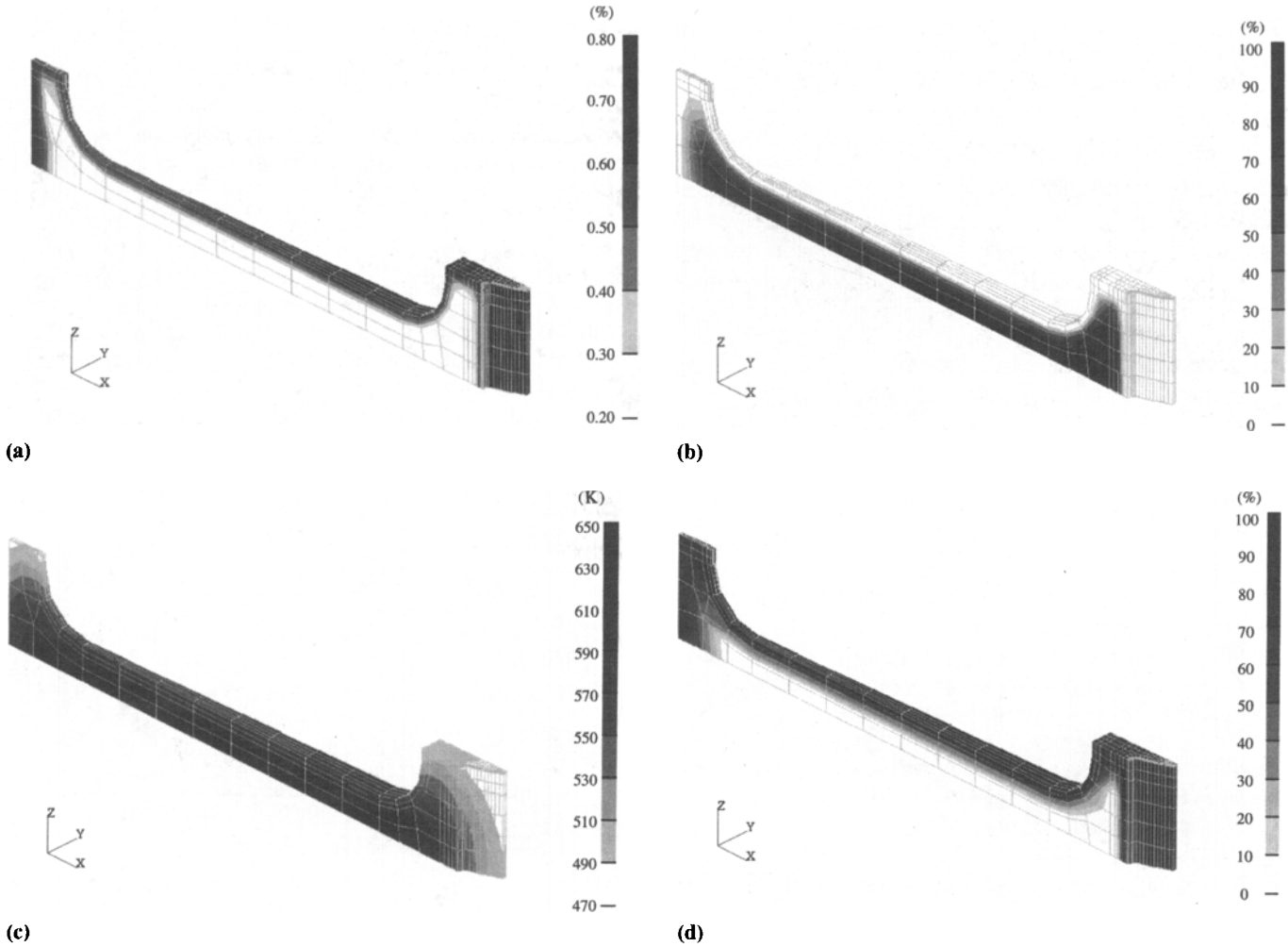

Fig. 8 Simulated results of carbon content, metallic structures, and temperature in the gear. (a) Carbon content after carburization. (b) Temperature during quenching (t = 30 s). (c) Volume fraction of bainite after quenching (d) Volume fraction of martensite after quenching

diffusion stage it is assumed that there is no carbon flux from external environments on any boundary. The boundary conditions for heat conduction analysis are such that convections from oil boundaries occur according to the heat transfer coefficient (2093.4 W/(m^{2}K)).

The simulated results are shown in Fig. 8 and 9. Figure 8(a) shows the distribution of carbon content after carburizing, and Fig. 8(b) illustrates the distribution of temperature during quenching (t = 30 s). Figures 8(c) and (d) depict the distribution of volume fraction of bainite and martensite after quenching, respectively. Residual stress distributions (axial, circumferential, and radial components) are represented in Fig. 9(a), (b), and (c), respectively. The fact that tensile residual stress in the circumferential direction is observed beneath the tip corresponds to practical experience with case-hardened gear, a decrease in bending fatigue strength. Figure 9(d) gives the enlarged deformation near the tooth after quenching.

4.3 *Induction Hardening of a Ring*

The induction hardening process can also be simulated by the HEARTS system (Ref 12). The model is a ring made of carbon steel with 100 mm in outer diameter, 50 mm in inner diameter, and 25 mm in height. The upper half of the ring is modeled as the axisymmetric problem. Induction heating is applied to the outer surface with an expected hardening depth of 2 mm during a 2.5 s heating period with 248 kW input power, followed by a cooling time of 15 s. The maximum temperature measured at the outer surface was 918 °C.

The heat generation during induction heating is assumed to occur 1.8 mm below the outer surface. The heat generation rate was determined by trial and error so that the maximum temperature at the surface reaches the measured value of 918 °C. The result reveals that uniform heat generation of approximately 4.6 × 10^9 W/m^3 is applied for 2.5 s in this case.

All surfaces are regarded as adiabatic boundaries during the heating process, while in the cooling process the outer surface is defined as the convection boundary with a uniform and constant convection coefficient of 3,000 W/(m^{2}K).

The simulated volume fraction of martensite on the symmetric surface between the upper and lower volumes of the ring are shown in Fig. 10 in comparison with the experimental hardness value. The mode of deformation after quenching is illustrated in Fig. 11, in which the numerical values at the tips of the

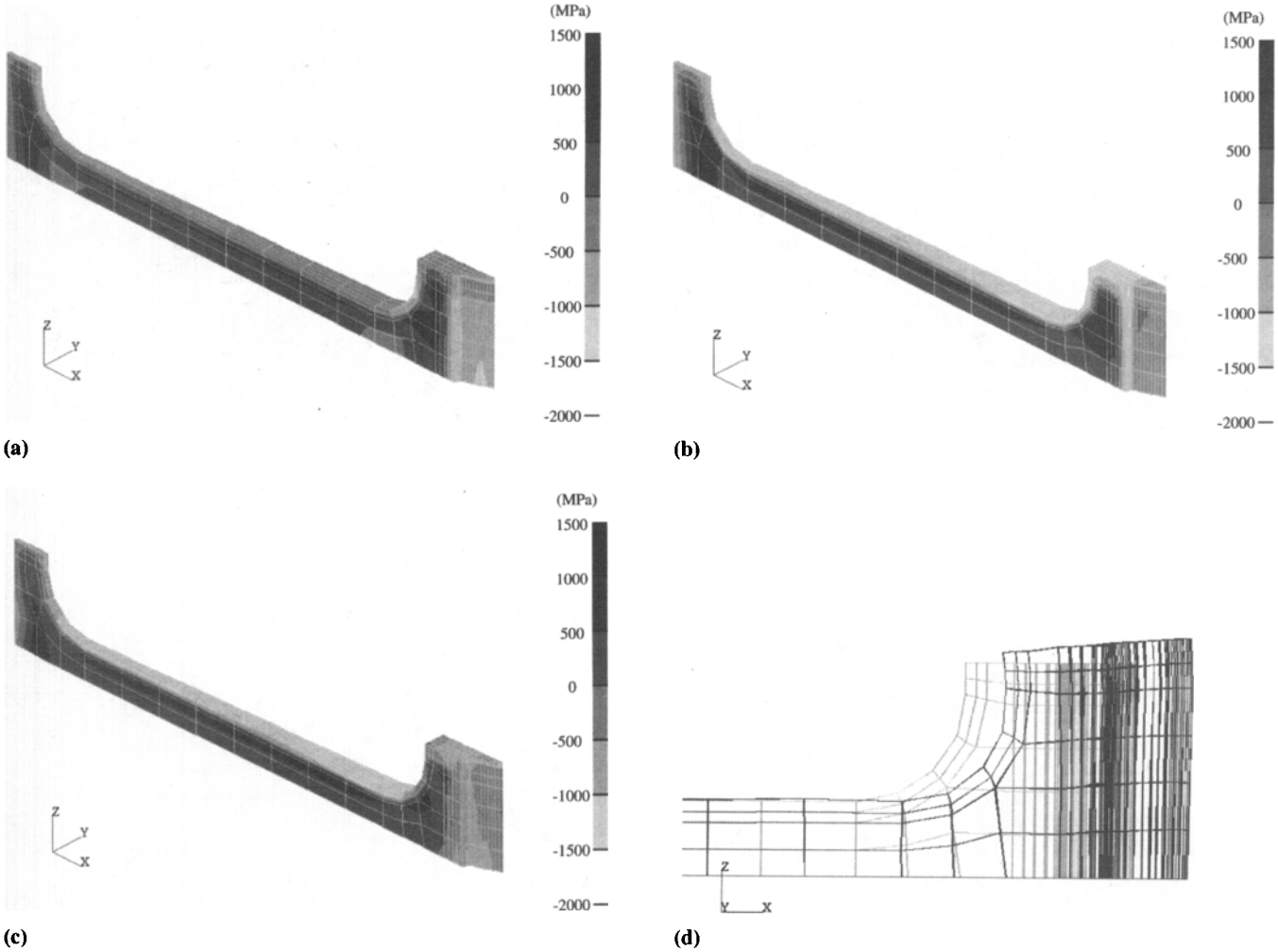

Fig. 9 Simulated results of residual stresses and distortion in the gear. (a) Axial stress. (b) Circumferential stress. (c) Radial stress. (d) Distortion near tooth

black triangles correspond to the measured values. The displacement of the ring shape toward the center is considered to be caused by the compressive plastic strain in the circumferential direction generated on the outer diameter near the surface.

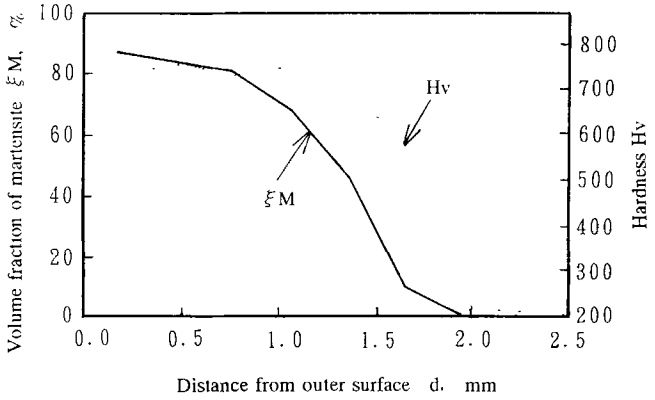

Fig. 10 Comparison between volume fraction of martensite and hardness in the ring

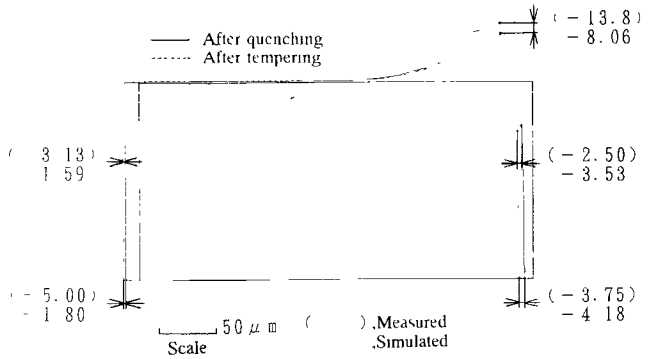

Fig. 12 Distortion after quenching and tempering of the ring

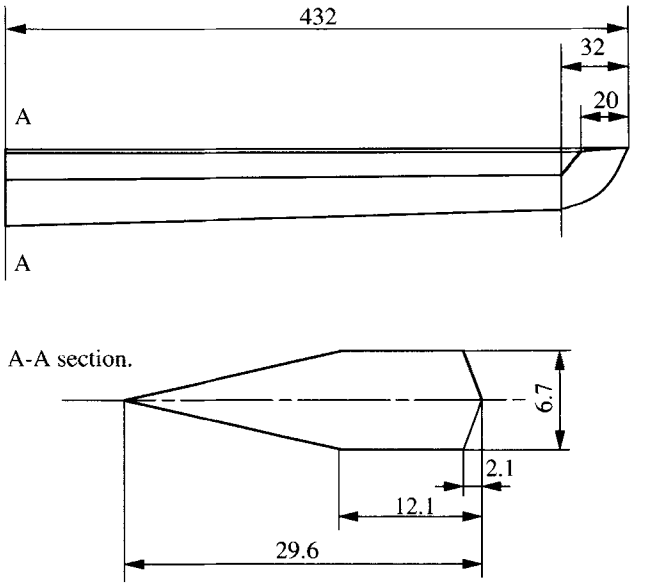

Fig. 14 Model of a sword, *Bizen-Osafune*

The tempering process of the quenched ring can also be simulated by the HEARTS system. The ring is kept at a steady temperature of 270 °C for 1 h after slow heating, followed by cooling to room temperature. At 80 to 160 °C, martensite is reduced to low-carbon martensite and ε-carbide, and the induced low-carbon martensite is resolved to ferrite and cementite at 260 to 360 °C. Figure 12 shows that tempering

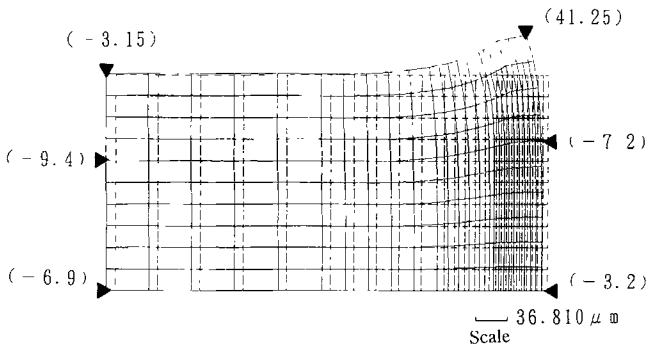

Fig. 11 Distortion after quenching in the ring

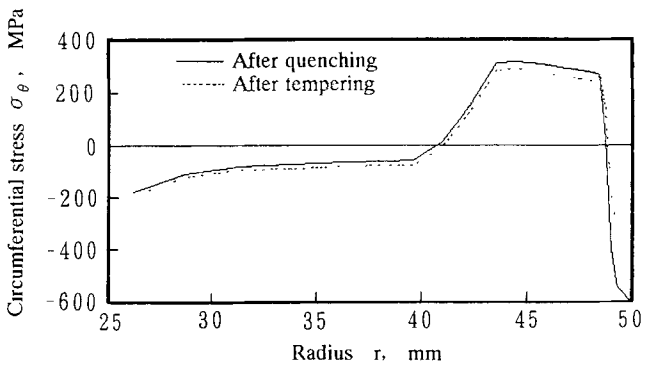

Fig. 13 Circumferential stresses after quenching and tempering of the ring

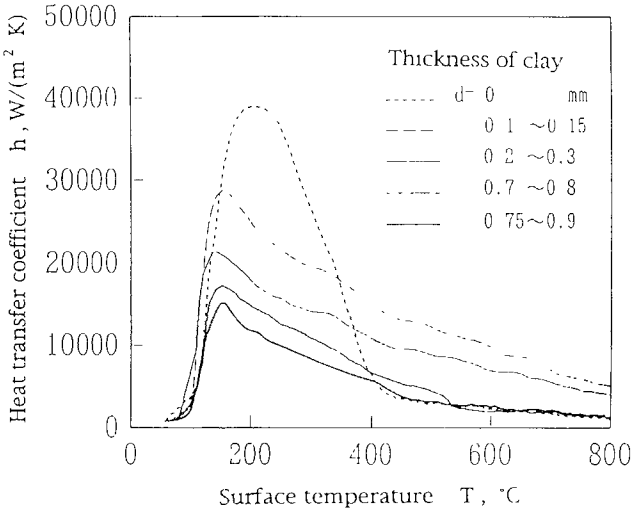

Fig. 15 Evaluated heat transfer coefficient in the sword depending on thickness of clay. Source: Ref 13

decreases the distortion at the upper surface and contracts the diameter of the ring.

Figure 13 shows the simulated distribution of circumferential residual stress before and after the tempering process on the symmetric plane. It follows that the compressive stresses near the outer surface decrease remarkably after the tempering process.

4.4 *Quenching of a Japanese Sword*

The final example treats the quenching process for a Japanese sword with the shape shown in Fig. 14, which is a model of a classical and famous sword, *Bizen-Osafune*. A 3-D finite element mesh division is made for half part in the width direction due to symmetry. There are 448 elements and 664 nodes. The model is composed of two kinds of materials: high-carbon steel in the blade part and low-carbon steel in the other part.

Before quenching, mixed clay with powders of charcoal and whetstone is pasted on the surface of the sword to control the heat transfer coefficient. The thickness is about 1.0 mm on the back and 0.1 mm on the blade. The relative heat transfer coefficient on the surface of the steel depends on the thickness of clay, as shown in Fig. 15. The sword is uniformly heated up to 850 °C and is quenched in water at 40 °C.

Figure 16 illustrates the temperature distribution of the sword with successive time from the beginning of quenching, and the mode of deformation. The thin part of the blade shrinks by thermal contraction due to severe cooling, which leads to the downward bending termed reverse bending. However, when martensitic transformation starts to occur in that part, normal bending again appears, because of the pearlitic transformation in the back side. In the successive stage, the back side shrinks

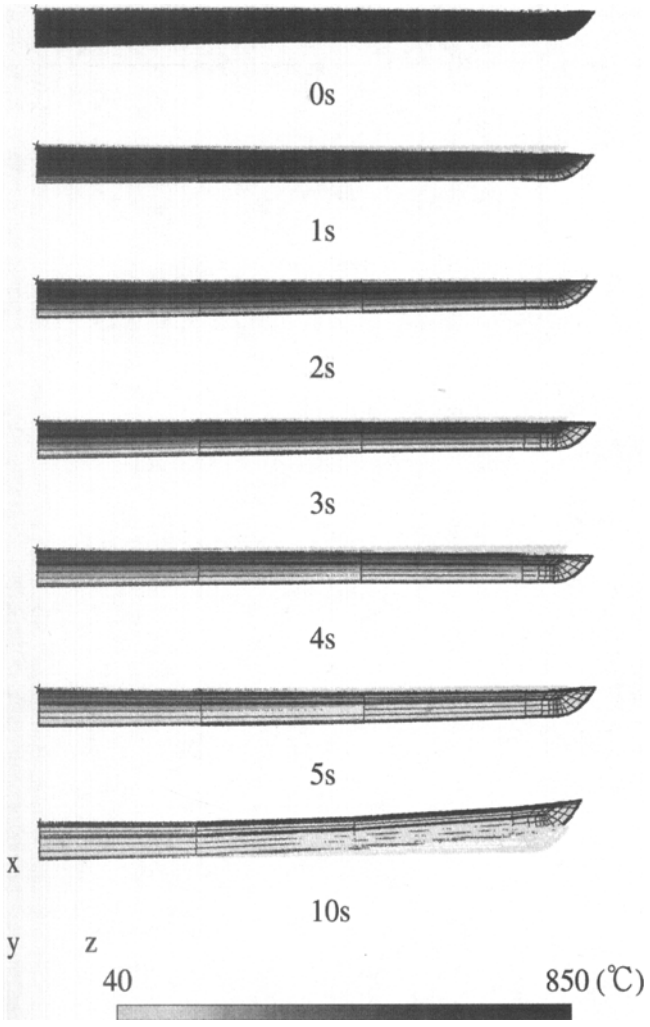

Fig. 16 Variation of distortion and temperature in the cooling process of the sword

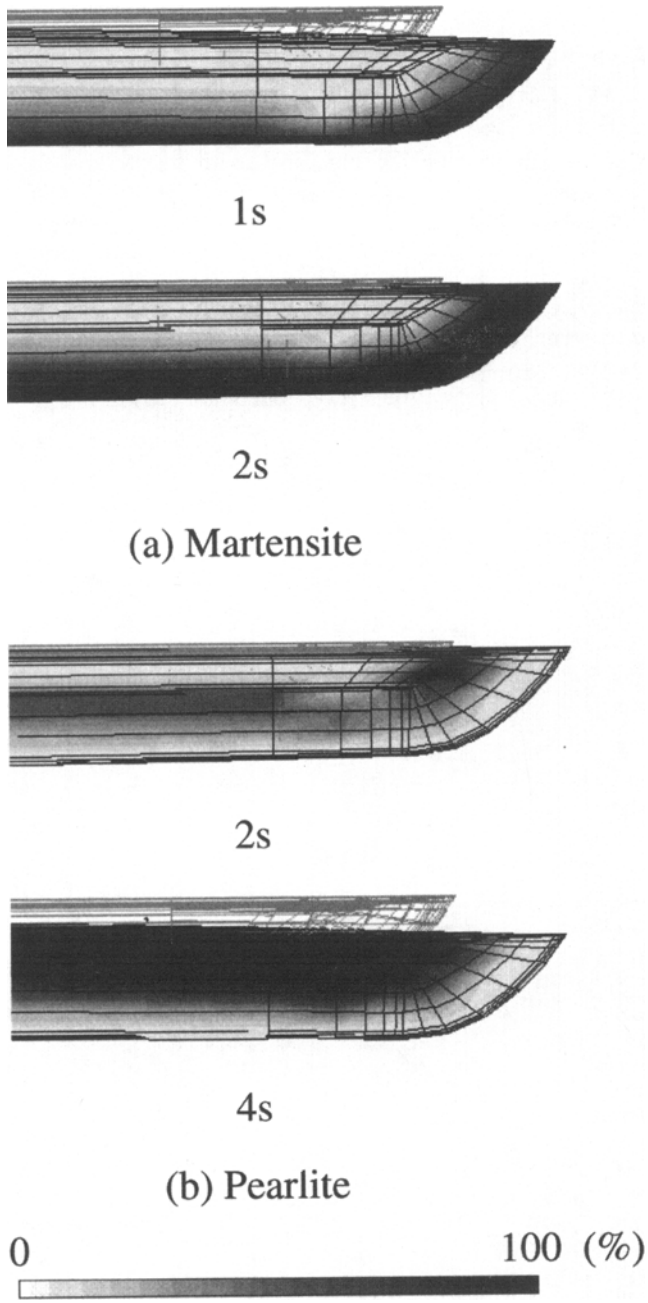

Fig. 17 Variation of distortion due to martensitic and pearlitic transformation in the sword

gradually because of thermal contraction, and finally normal bending can be obtained owing to the difference in the coefficient of dilatation by martensitic and pearlitic transformation, as shown in Fig. 17.

5. Conclusion

The current version of the HEARTS system is limited to the heat treatment process. However, other types of phase transformations, such as melting and solidification, are essential in welding, casting and so on, and we expect to include these processes by modifying the constitutive and rate equations.

Acknowledgments

The HEARTS system has been developed by the joint work of many collaborators. The authors especially express their gratitude to Professor K. Tanaka, Tokyo Metropolitan Institute of Science and Technology, and Professor S. Nagaki, Okayama University, for their work in the construction of the theory. Acknowledgment is also due to Dr. Z.G. Wang, graduate student of Kyoto University, now at the University of British Columbia, and Dr. D.Y. Ju, Saitama Institute of Technology, for development of the prototype programs, and to users of the HEARTS system, especially Mr. F. Ikuta, Neturen Co., Ltd., for evaluation of the system and collection of material data.

References

1. T. Inoue and K. Tanaka, *J. Soc. Mat. Sci., Japan,* Vol 22, 1973, p 218 (in Japanese)
2. T. Inoue, S. Nagaki, T. Kishino, and M. Monkawa, *Ing.-Arch,* Vol 50, 1981, p 315
3. T. Inoue and B. Raniecki, *J. Mechanics and Physics of Solids,* Vol 26, 1978, p 187
4. Z.G. Wang and T. Inoue, *J. Soc. Mat. Sci., Japan,* Vol 32, 1983, p 991
5. T. Inoue, K. Arimoto, and D.Y. Ju, *Proc. First Int. Conf. Quenching and Control of Distortion,* ASM International, 1992, p 205
6. T. Inoue, et al., *The Phase Transformation and Numerical Simulation of Material Behavior,* Korona Inc., Japan, 1991 (in Japanese)
7. T. Inoue, K. Tanaka, and S. Nagaki, *Solid Mechanics and Analysis of Transformation,* Taiga Publishing, Inc., Japan, 1995 (in Japanese)
8. W.A. Johnson and F.R. Mehl, *Trans. AIME,* Vol 135, 1939, p 416
9. C.L. Magee, *Phase Transformation,* ASM International, 1968, p 115
10. G.W. Greenwood and R.H. Johnson, *Proc. Roy. Soc. London,* Vol 283A, 1965, p 403
11. K.J. Bathe, *Finite Element Procedures in Engineering Analysis,* Prentice-Hall, Inc., 1982
12. K. Arimoto, F. Ikuta, and T. Inoue, *J. Japan Soc. Heat Treat.,* Vol 34, 1994, p 332
13. H. Kanamori, H. Uchida, S. Koyama, E. Nakamura, and T. Inoue, *Preprints of the 37th Annual Conference of the Society of Heat Treatment Technology,* Japan, 1993